Supplementary information.

Thermal decomposition.

In a first approach, we selected the conditions previously optimized in the group for the synthesis of iron-nickel nanoparticles. We thus attempted a classical thermal decomposition. **1** was used as the cobalt precursor. The two organometallic precursors (1mmol each) were reacted in toluene at reflux (in the presence of an amine, here 1mmol hexadecylamine (HDA), as a stabilizing agent (**sample 1**). A black material (570mg) was obtained after evaporation of the solvent. Elemental analysis evidences an iron rich composition with a Fe/Co ratio of 1.5 ($Fe_{60}Co_{40}$). Transmission Electron Microscopy (TEM) investigations show that the product obtained is composed of 7.4(σ = 0.2) nm non spherical particles displaying a very irregular shape and important surface oxidation (Figure 1A).

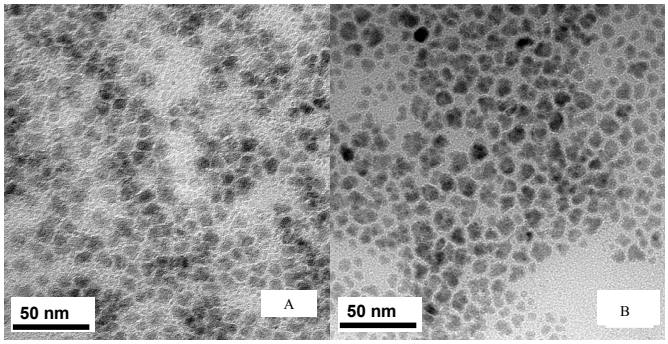

Fig 1 TEM micrographs: A) Sample 1; B) Sample 2.

Energy Dispersive X-Ray analysis (EDX) of a few nanoparticles confirms that they are iron rich (Fe/Co = 1.39). In a second attempt, we selected a ligand system previously demonstrated to lead to a nearly perfect control of the size distribution of Co[1] or Fe[2] nanoparticles and of certain bimetallic Co based nanoparticles[3], i.e. a mixture of long chain carboxylic acid and amine. The decomposition has been first carried out in the presence of 1mmol oleylamine and 1mmol oleic acid (OA), while keeping the metal precursors quantities identical (1mmol each). The temperature was set to 150°C, to facilitate the decomposition of possible intermediate carboxylate complexes which may form in such a medium. The product obtained after 2 hours of reflux consists of macroscopic needles agglomerated on the magnetic bar (**sample 2**) that could be isolated by filtration. The composition of the material, $Fe_{18}Co_{82}$, was determined by EDX on one nanoparticle. It confirms the bimetallic character of the nanoparticles with a Fe/Co ratio of 0.22 in perfect agreement with the elemental analysis. In this case, the average size of the particles determined from the TEM observation is 11 nm (Figure 1B). However, the size distribution is rather broad (2-25nm) and the shape of the nanoparticles is not controlled. Furthermore, the metal composition is far from the targeted one, and the yield is very low (no more than a few mg could be collected). This is probably a consequence of the kinetics of decomposition of the precursors as will be addressed in the discussion part of this paper. In summary, both experiments led in poor yield to particles polydisperse in size and shape, with partial oxidation of their surface.

Variation of the ligands.

In order to investigate how a variation of the ratio and nature of the ligands modifies the material, a study was carried out using both precursor systems, namely $[Fe(CO)_5]$ and $[Co(\eta^3\text{-}C_8H_{13})(\eta^4\text{-}C_8H_{12})]$ on one side, and $[Fe(CO)_5]$ and $[Co(N(Si(CH_3)_3)_2)_2]$ on the other, leading respectively to **samples 8-13** and **14-17** in the presence of different ligand sets. The general conditions were those used hereabove, namely 150°C and $[Co(\eta^3\text{-}C_8H_{13})(\eta^4\text{-}C_8H_{12})]$ as precursor for **samples 8-13** and 150°C and $[Co(N(Si(CH_3)_3)_2)_2]$ as precursor for **samples 14-17**.

In the first group, the use of an amine of shorter chain (dodecylamine, DDA) instead of HDA has been tested (**sample 8**) without any change in the mean size of the nanoparticles. Linear saturated carboxylic acids of chain lengths C_{16} (palmitic acid, PA) and C_{18} (stearic acid, SA) have been used instead of OA which displays a kinked C_{18} chain due to the *cis*-configuration of the double bond in the C_9 position (respectively **samples 9** and **10**). TEM images showed that the size distribution observed for **sample 10** resembles that of the reference **sample 6,** whereas the one obtained for **sample 9** is much broader. We also tried to increase the acid/amine ratio up to 2 (**samples 11** and **12**) or to increase the overall quantity of stabilising agent compared to the quantity of precursor used by a factor of 2 (**sample 13**) leading to nanoparticles displaying a broad size distribution with sizes varying between 10 and 100 nm. Despite the differences in average size, size distribution and shape of the nanoparticles, they arrange into millimetre long black solids which display a composition close to the target composition ($Fe_{60}Co_{40}$), as well as metal weight fractions varying from 70 to 85% depending on the ligand set used (Table 1).

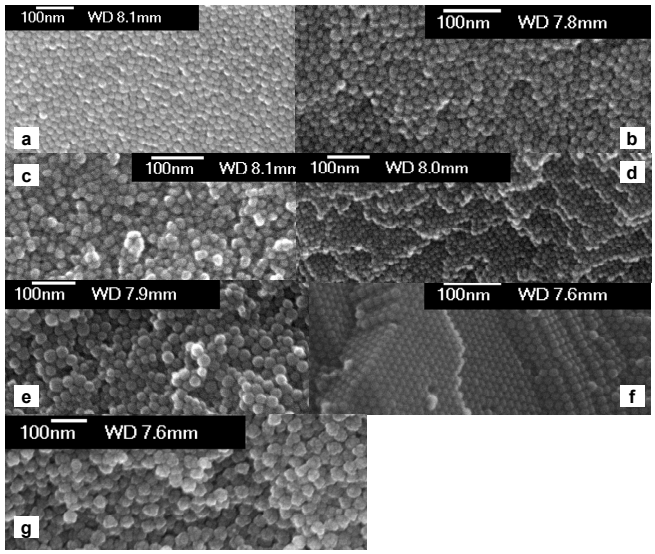

Fig. 2 SEM-FEG micrographs of : a) Sample 6; b) Sample 8; c) Sample 9 d) Sample 10; e) Sample 11; f) Sample 12; g) Sample 13.

These solids were directly collected from the reaction vessel and observed by SEM-FEG (Fig. 3). For most of the samples (**samples 6, 8, 10, 11, 12**), the nanoparticles inside these solids are organized into ordered super-structures. In the case of **sample 6**, sharp ridges induced by the SEM-FEG vacuum revealed the inner organization of the solids showing close-packed self organized particles within millimeter sized superstructures. TEM experiments, performed on thin samples prepared by ultra-microtomy confirm the hexagonal 2D packing of 15 nm diameter monodisperse nanoparticles. Inset Fig. 3 is a Fourier Transform (FT) performed on the whole TEM images.

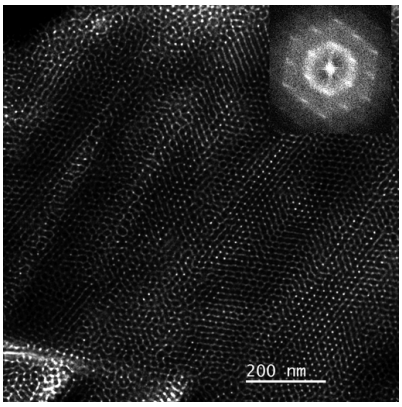

Fig. 3 TEM micrograph of sample 6 after ultra-microtomy. Inset : Fourier Transform of the whole picture.

The discrete reflections and the 6 fold symmetry of the FT indicate that this regular organization remains at least over regions as large as 1 micron even if several stacking faults can be observed. Due to the large parameter of the super-crystal (~15 nm), its symmetry is difficult to elucidate by electron diffraction techniques. Interestingly, an optimization of the organisation process is achieved when using one extra equivalent of stearic acid (**Sample 10**), leading to very large super-crystals of otherwise totally similar particles. In this case, the organization is also visible throughout the super-crystals and local fcc packing is revealed by SEM on a broken super-crystal. The regularity of the precipitated structure is attributed to the monodispersity of the particles.

In the second group (**samples 14-17**), consisting of the particles synthesized from $[Fe(CO)_5]$ and $[Co(N(Si(CH_3)_3)_2)_2]$, PA and SA saturated acids of chain lengths C_{16} and C_{18} have also been used instead of OA (respectively **samples 14** and **15**) but no change in the average size or size distribution of the nanoparticles could be evidenced by TEM. Similarly, an amine of shorter chain (DDA) was used in association with OA (**sample 16**). Here again both size and size distribution were identical to those of the reference **sample 7**. Finally, a 2/1 HDA/OA ratio was used (**sample 17**), which led to an assembly of nanoparticles polydispersed in size (15-50 nm). In each case, a black powder was obtained in high yield (above 85% on cobalt) at the end of each reaction, which could be isolated by filtration.

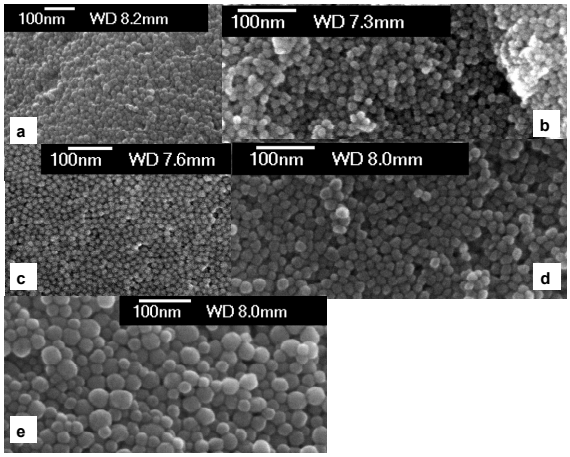

Fig. 4 SEM-FEG micrographs of : a) Sample 7; b) Sample 14; c) Sample 15; d) Sample 16; e) Sample 17.

SEM-FEG observations of **samples 7, 14, 15, 16** (Fig. 4) evidenced the presence of large super-structures of particles of 15 nm mean diameter and displaying a narrow size distribution. Despite the apparent densely packed assembly of the particles, no clear long range organization was detected, apart for **sample 14**, which looks slightly more organized than the others. The main characteristics of these systems are reported in Table 2.

Table 1. Syntheses from $[Fe(CO)_5]$ and $[Co(\eta^3\text{-}C_8H_{13})(\eta^4\text{-}C_8H_{12})]$ under H_2 presssure

Sample name	Ligands used	Microscopy observation	Metal weight fraction (recovered mass)
6	1 HDA + 1OA	Monodispersed 15nm spherical particles, very dense packing.	75.0%
8	1 DDA + 1 OA	Monodispersed 15nm spherical particles. Very similar to sample 8.	81.7%
9	1 HDA + 1 PA	Particles of various size and shapes.	79.0%
10	1 HDA + 1 SA	Monodispersed 15nm spherical particles. Very similar to sample 8 and 9.	81.5%
11	1 HDA + 2 OA	30 nm particles non monodispersed in size nor shape.	78.4%
12	1 HDA + 1OA + 1SA	Monodispersed 15nm spherical particles organized in 3D superlattices.	84.5%
13	2 HDA + 2 OA	40nm particles, non monodispersed in size nor shape.	80.5%

Table 2. Syntheses from $[Fe(CO)_5]$ and $[Co(N(Si(CH_3)_3)_2)_2]$ under H_2 pressure:

Sample name	Ligands used	Microscopy observation	Metal weight fraction(recovered mass)
7	1 HDA + 1OA	Monodispersed 15nm spherical particles, very dense packing. No organization.	80.0%
14	1 HDA + 1 PA	Monodispersed 15nm spherical particles, very dense packing. No organization. Very similar to sample 7 and 15.	81.5%
15	1 HDA + 1 SA	Monodispersed 15nm spherical particles, very dense packing. More organized packing.	77.2%
16	1 DDA + 1 SA	Monodispersed 15nm spherical particles, very dense packing. No organization. Very similar to sample 7.	85.1%
17	2 HDA + 1OA	15-50 nm polydispersed particles.	79.0%

Supplementary Material (ESI) for Journal of Materials Chemistry

Magnetic properties.

Sample name	Ms[a]	μ	μ_0Hc[b]
1	100	$1.04\mu_B$	0.039
3	130	$1.4\mu_B$	0.0025
4	130	$1.4\mu_B$	0.0040
6	160	$1.71\mu_B$	0.0100
7	183	$1.95\mu_B$	0.0100
9	135	$1.43\mu_B$	0.0010 (300K)
10	182	$1.94\mu_B$	0.0070
11	169	$1.87\mu_B$	0.0125
14	120	$1.28\mu_B$	0.0041 (300K)
17	113	$1.20\mu_B$	0.007 (300K)

Table 3. Magnetic properties of some representative samples. [a] values in $A.m^2.kg_{FeCo}^{-1}$; [b] values in T at 2K (except when précised).

[1] F. Dumestre, B. Chaudret, C. Amiens, M. Respaud, P. Fejes, P. Renaud and P. Zurcher, *Angew. Chem. Int. Ed,.* 2003, **42**, 5213.

[2] F. Dumestre, B. Chaudret, C. Amiens, P. Renaud and P. Fejes, *Science,* 2004, **303**, 821.

[3] E. V. Shevchenko, D. V. Talapin, A. L. Rogach, A. Kornowski, M. Haase and H. Weller, *J. Am. Chem. Soc.,* 2002, **124**, 11480.